JOINT EUROPEAN TORUS

JET–P(92)57

D.P. O'Brien, J.J. Ellis, J. Lingertat
and JET Team

Local Expansion Method for Fast Plasma Boundary Identification at JET

Local Expansion Method for Fast Plasma Boundary Identification at JET

D.P. O'Brien, J.J. Ellis, J. Lingertat
and JET Team*

JET-Joint Undertaking, Culham Science Centre, OX14 3DB, Abingdon, UK

** See Annex*

Preprint of Paper to be submitted for publication in
Nuclear Fusion

LOCAL EXPANSION METHOD FOR FAST PLASMA BOUNDARY IDENTIFICATION AT JET

D.P. O'Brien, J.J. Ellis, J. Lingertat

JET Joint Undertaking, Abingdon, Oxon, OX14 3EA, U.K.

Abstract

A local expansion technique for the reconstruction of the plasma boundary is presented. The method is particularly accurate in identifying the separatrix in X-point configurations. It is applied to JET discharges and the results compared with those of a full equilibrium code and with other independent diagnostics. It is found that the majority of the H-mode discharges at JET have been achieved in marginal limiter configurations. The method is sufficiently reliable and fast for real time shape control.

1. Introduction

The importance of the physical mechanisms, operating at the plasma edge, in determining the overall performance of fusion devices has become increasingly recognised in recent years [1], especially so with the advent of the H-mode high performance regime of operation observed on tokamak machines [2]. The improved confinement region obtained in this mode of operation is known to originate at the plasma edge [3], and as many of the edge physics diagnostics and models are sensitive to errors in the determination of the plasma boundary this can lead to contradictory results in the description of the H-mode [4]. The accurate determination of the magnetic field configuration close to the plasma boundary of present day tokamak devices has therefore become increasingly important.

We describe here a local expansion technique to determine the complete plasma boundary. In the past, scepticism has been expressed concerning the use of Taylor series type expansions in global plasma boundary determinations [5,6,7]. Previous expansions have been restricted in the most part to a very local region in the vicinity of the measurements, the main application being for plasma position control [8]. The 'local' method used at JET and described here makes use of five 6th order expansions of the flux function which are symmetric in major radius and constrained by the vacuum field equations. By fitting to the local field and flux measurements they can give an accurate determination of the boundary in the vicinity of the measurements. The expansion in the region of an X-point for separatrix configurations is particularly suitable in localizing the X-point. By constraining adjoining fits to match at chosen "tie" points a global reconstruction of the plasma boundary is obtained. In line with the philosophy of the method these constraints are applied in a least squares sense. The method is sufficiently reliable and fast for real time shape control.

2. Local Expansion Technique

The local expansion method was originally introduced at JET in order to have a fast and accurate determination of the plasma boundary in the neighbourhood of

an X-point. It has been extended to cover the whole plasma boundary and is now used for arbitrary plasma configurations. The basis of the method is five sixth order expansions of the poloidal flux, one each, at the top, bottom, inboard, upper belt and lower belt limiters of the vessel. The expansions are given by

$$\psi(R,Z) = \sum_{\substack{i=0 \\ j=0 \\ i+j\le 6}}^{6} a_{ij}\rho^i z^j \qquad (1)$$

where $\rho = R^2 - R_0^2$, $z = Z - Z_0$, and (R_0, Z_0) is the centre of the expansion. The variable ρ rather than $R - R_0$ is chosen because of the symmetry of the Grad-Shafranov equation about the major axis of the torus (R=0). The coefficients a_{ij} are determined by imposing the vacuum equation

$$\Delta^*\psi = 0; \quad \Delta^* = \partial_{RR} + \partial_{ZZ} - \frac{1}{R}\partial_R \qquad (2)$$

and by fitting to the local flux and magnetic field measurements. In addition the five expansions are constrained to match at chosen tie points around the vessel.

Having imposed the vacuum equation, each expansion is left with 13 independent coefficients to be determined, leading to a total number of 65 coefficients for the 5 expansions. The flux and magnetic field may be written in terms of these coefficients as

$$\begin{aligned} \psi_c^\alpha(\rho,z) &= \sum_{i=1}^{13} \psi_i^\alpha(\rho,z)\, C_i^\alpha \\ B_c^\alpha(\rho,z) &= \sum_{i=1}^{13} B_i^\alpha(\rho,z)\, C_i^\alpha \qquad \alpha = 1 \ldots . 5 \end{aligned} \qquad (3)$$

where B_c refers to the component of $\underline{B}$ in the direction of the measuring coil. If no ties between the expansions are used each fit is independent, giving rise to 5 least squares calculations from minimising

$$\begin{aligned} \chi_\alpha^2 &= \tfrac{1}{2} \sum_{\substack{Flux \\ loops}} w_j^\alpha \left(\psi_m^\alpha(j) - \psi_c^\alpha(j)\right)^2 \\ &+ \tfrac{1}{2} \sum_{coils} w_j^\alpha \left(B_m^\alpha(j) - B_c^\alpha(j)\right)^2 \end{aligned} \qquad (4)$$

with respect to the C_i^α where (ψ_m, B_m), (ψ_c, B_c) are the measured and calculated values of the flux and field at the measuring points (R_j, Z_j). The five fits may be combined to the equivalent minimization of

$$\chi^2 = \tfrac{1}{2} \sum_{j=1}^{N_m} w_j \left(m_j - \sum_{i=1}^{65} d_{ji} C_i\right)^2 \qquad (5)$$

where m_j are the measurements and $d_{ji} \equiv \psi_i^{\alpha}(\rho_j, z_j)$ etc. For each j only 13 of the d_{ji} are non-zero. Each physical measurement may occur in more than one expansion so the m_j are not necessarily distinct. The minimization may be summarized as

$$DC = M^* \tag{6}$$

where

$$D_{ki} = \sum_{j=1}^{Nm} w_j d_{ji} d_{jk}$$

$$M_k^* = \sum_j w_j d_{jk} m_j \tag{7}$$

We see that D consists of 5 'diagonal blocks' of 13×13 matrices $D(\alpha)$ of the form

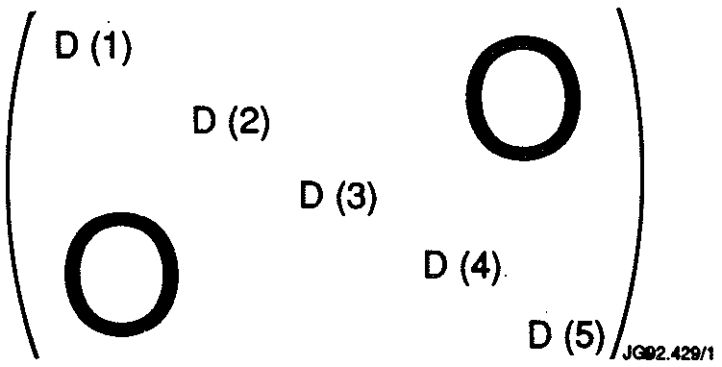

The choice of 6th order for the expansion and the use of 5 fits is a compromise: The accuracy of the results (judged by comparison with an equilibrium code) improved as the order of the expansion and the number of fits was raised, but the number of measurements needed also increased. The truncation errors associated with a Taylor expansion become worse as the distance from the centre of the expansion increases, and so the use of measurements far from $\rho = 0, z = 0$ in the least squares fit results in a decrease in the accuracy of the answer. To overcome this problem additional constraints were introduced between neighbouring expansions such that the flux at given points were made to agree. These "tie" points were chosen mid way between the expansion centres (where the errors from both expansions are comparable), in groups (to match the flux and its derivatives), and in a region outside the plasma. By this means the maximum distance of a measurement from the corresponding centre could be reduced. Initially neighbouring expansions were constrained to agree exactly at these "hard tie points".

It was found that results could be improved (especially with small plasmas) by relaxing the constraint that adjacent expansions match exactly, but allow an error term $w_j (\psi^{\alpha}(R_j,Z_j) - \psi^{\beta}(R_j,Z_j)^2$ to be included in the expression to be minimised. These so called soft ties between the fits are implemented by introducing additional measurements $m_j = 0$ at points (R_j, Z_j) where the ties are to be imposed and defining additional matrix elements $d_{ji} \equiv d(1)_{ji} - d(2)_{ji}$, where i is the coefficient index, j labels the tie point (R_j, Z_j), and d(1), d(2) refer to the two fits involved in the tie. This procedure introduces non-zero off diagonal blocks into

the block matrix D described above; the method of solution remains the same but a 65 × 65 matrix must now be inverted.

When inaccurate data is suspected, hard ties are introduced to constrain two neighbouring fits to match exactly at a point (R_j, Z_j). A constraint between fits 1 and 2 would have the form

$$\sum_{i=1}^{65} d_{ji}(1)C_i = \sum_{i=1}^{65} d_{ji}(2)C_i \qquad (8)$$

Hence each hard tie point enables one of the 65 coefficients to be eliminated from the calculation, so that we can write

$$AC^h = BC^r \qquad (9)$$

where the 65 coefficients C are divided into n_h coefficients C^h, which are eliminated from the minimization process, and 65-n_h coefficients C^r. The coefficients in C^h are chosen so that A is non-singular giving

$$C^h = A^{-1}BC^r \qquad (10)$$

and a matrix T can be constructed where

$$C = TC^r$$

If we substitute this expression for C into χ^2 and minimize w.r.t. C^r this is equivalent to replacing $\sum_{i=1}^{65} d_{ji}\, C_i$ by $\sum_{i=1}^{65-n_h} d^*_{ji}\, C^r_i$ where $d^*_{ji} = \sum_{k=1}^{65} d_{ji}\, T_{ki}$. This leads to a minimization given by an equation of the type (6).

Without any tie point constraints, each expansion requires at least 13 measurements to give a solution. Presently the JET magnetic measurement system just about satisfies this criteria. There are plans to increase the number of available measurements, which will give a more robust reconstruction. The plasma boundary is found in the usual way by finding the minimum flux value (the plasma current in JET is negative) between various limiter components around the vessel as well as at any separatrices if they exist inside the vessel. Any X-points of the poloidal field B_p are found using a Newton-Raphson procedure to solve $\nabla\psi = 0$.

3. Benchmark Calculations

In order to benchmark the method we reconstruct the plasma boundary for various plasma configurations, using magnetic data generated by the full equilibrium code IDENT [9]. The usual magnetic field measurements at JET are used. They consist of a maximum of 34 magnetic coils and 14 flux loops placed around the wall of the vessel. There is a higher density of magnetic coils at the top and bottom of the vessel in regions where X-points of the field are formed. In these regions we also measure two perpendicular components of the magnetic field in order to give a more accurate location for X-points.

The comparison between the numerically generated boundaries of IDENT and the reconstructed boundaries using the local expansion method XLOC are shown in Fig. 1. We see that for all configurations there is good agreement with an error of less than 2% (~ 2 cm) of the minor radius for the whole boundary. Given that the grid size in IDENT is of the order of 7 cm, this discrepancy could easily be absorbed into the inaccuracy of the numerical scheme underlying IDENT.

For the proposed pumped divertor, which will become operational in 1993 [10] we reconstruct the plasma boundary using magnetic data generated by the full equilibrium code EFITJ [11]. The magnetic field measurements are now 44 magnetic coils and 27 flux loops. The comparison between the EFITJ boundary and the reconstructed boundary using XLOC is shown in Fig. 2.

4. Experimental Results

The local expansion method of plasma boundary reconstruction has been run continuously during operations at JET for the past three years. We have extracted data from the JET data base system in order to make comparisons with other boundary diagnostics. The results are presented below.

4.1 Comparison with IDENT

The distances CR1-CR6 used to characterize the plasma boundary are shown in Fig. 1a. They are respectively the distance to the inner wall, RF antenna upper belt limiter, lower belt limiter, upper inner wall and lower inner wall. The comparison of these distances between the reconstructed boundary from XLOC and the reconstructed boundary from IDENT are shown in Fig. 3 in the form of a scatter plot, using data from the 1990 to 1992 JET experimental campaigns. We see that there is generally good agreement especially when the plasma to vessel component distance is less than 10 cm.

4.2 Comparison with independent diagnostics

The standard interpretation of the divertor diagnostics uses the magnetic configuration given by XLOC in the divertor region. However for some discharges it is possible to use raw measurements from these diagnostics to check the accuracy of XLOC. The divertor diagnostics which are used for this purpose are the Langmuir probes installed in the target plates and the CCD Camera recordings of the light emission from the target plates.

If the X-point of a discharge is swept across the target tiles so that the strike points of the separatrix cross over a Langmuir probe, this will result in changes in the Langmuir characteristics. Although the detailed physics of the rapid changes in the plasma parameters which occur at the transition between the scrape-off layer and the private flux region are not fully understood, it is reasonable to assume that the transition takes place where the major changes in the Langmuir characteristics occur. Fig. 4 shows the radial position of the inner and outer magnetic strike points given by XLOC as a function of time for two hot-ion upper X-point discharges. The radial position of two probes is also given. According to Fig. 4 both probes are crossed by both strike points for shot 26019, whereas for

shot 26021 only probe 2 is approached. Figs. 5 and 6 show the floating voltage U_f of the probes as a function of the strike point position R_{XLOC}. The floating voltage is an unprocessed parameter taken directly from the measured Langmuir characteristics. We see that there is a clear and distinct change of the floating voltage within a narrow region ΔR_{XLOC} of the major radius (ΔR_{XLOC} = 5 - 12 mm). It is assumed that this change is the result of the strike point crossing over the respective probe. This assumption is supported by the fact that the plasma parameters obtained after processing the Langmuir characteristics (n_e, T_e) undergo similar changes in the same interval ΔR.

On the CCD camera recordings of the light emission from the target plates very well localised hot spots can be observed. Generally, they are located on tiles that have a larger inclination against the magnetic field (ski slopes) than the flat surface of the plates. The location of the hot spots should be at the maximum of the parallel heat flux, i.e. just at the strike points of the separatrix [12]. From the tape recordings of the shots 26019 and 26021 the radial co-ordinate R_{CCD} of the hot spot at the outer strike points has been visually determined relative to geometric features of the target tiles (edges, bolt holes). This method was used only in time intervals where the radial width of the hot spot was less than 1 cm and the estimated accuracy of this procedure is ± 1 cm. The values obtained, together with the corresponding radial position of the strike point according to XLOC, R_{XLOC}, are given in Fig. 7. Fig. 7 shows a scatter of the measured points around the straight line of ideal agreement between both methods. The maximum deviation from the straight line is 16 mm, the mean deviation is 10 mm.

Both these methods give comparable values of accuracy (± 10 mm) for XLOC. The Langmuir probe results show a systematic difference between XLOC and the positions of the probe, whereas the CCD results show a random scatter. It seems that the assumed accuracy of the CCD method is overestimated and that the Langmuir probe results are more representative.

Spectroscopic measurements can also be used to assess the accuracy of the boundary reconstruction. As the plasma changes configuration from outboard limiter to divertor to inner wall limiter so the neutral H flux as measured by the H_α bremstrahlung in these positions will rise and fall. Fig. 8 shows the configuration obtained by XLOC as a function of time (RF-antenna limiter = 4, lower belt limiter = 2, upper X-point = 0, inner wall limiter = 8) with the various H_α signals plotted beneath. We see that the transitions RF-antenna lower belt - RF-antenna lower belt - upper X-point - inner wall obtained by XLOC are simultaneous with the variations in the H_α signals in the appropriate region.

4.3 H-mode

The results obtained from XLOC for the position of the X-point showed that prior to the end of 1990 most of the H-modes achieved at JET were "marginally limited" with the X-point outside the vessel and the plasma limited on the carbon tiles in the divertor region. Subsequently magnetic configurations were obtained with the X-point well inside the vessel. These results are summarised in Fig. 9. The affect of X-point position on confinement is discussed in [13], the main conclusion being that the diamagnetic stored energy scales more weakly

with I_p than linearly as the X-point moves further outside of the vessel with increasing current.

5. Summary

The XLOC boundary reconstruction package is in routine use at JET and has an accuracy in localizing X-points of < 2cm. Its boundary has been compared with the boundary of the full equilibrium identification code IDENT showing excellent agreement at the inboard and outboard sides of the plasma. However it gives a more accurate X-point location when comparisons are made with other diagnostics such as the Langmuir probes in the X-point region, and the strike zones obtained from the CCD camera observations. This more accurate determination of the X-points has shown that H-modes at JET can be obtained with a marginally limited configuration as well as in true X-point configurations with the X-point inside the vessel.

Acknowledgement

The authors would like to thank Prof. K. Lackner, Dr. J.G. Cordey and Dr. J.P. Christiansen for stimulating discussions. We would also like to thank M. Lesourd who provided the CCD camera observations.

References

[1] Stangby, P.C., McCracken, G.M., Nucl. Fusion, 30, No. 7 (1990) 1225.

[2] Wagner, F., et al., Nucl. Fusion 25 (1985) 1490.

[3] Asdex Team, Nucl. Fusion 29 (1989) 1959.

[4] Harbour, P.J., Loarte, A., JET P(92) 32.

[5] Lee, D.K., Peng, Y., K.M. Peng, J. Plasma Physics 25 (1981) 161-173.

[6] Braams, B.J., "The Interpretation of Tokamak Magnetic Diagnostics. 'status and prospects', IPP 5/2 1985.

[7] Hofmann, F., Tonetti, G., Nucl. Fusion 28 (1988) 519.

[8] Bertolini, E., Mondino, P., Noll, C.P., Fusion Technology 11, No. 1 (1987) 71-119.

[9] Blum, J., Lazzaro, E., O'Rourke, J., Keegan, B., Stephan, Y., Nucl. Fusion 30 (1990), 1475.

[10] Rebut, P.H., et al., JET-R (89) 16.

[11] O'Brien, D.P., et al., 17th Eur. Conf. Fusion Plasma Heating, Amsterdam, ECA 14B part 1 (1990), 251.

[12] Loarte, A., Harbour, P., Nuclear Fusion 32, 104 (1992) 681.

[13] Jones, T.T.C., et al., 19th Eur. Conf. on Controlled Fusion and Plasma Physics, Innsbruck, 16C part 1 (1992), 3.

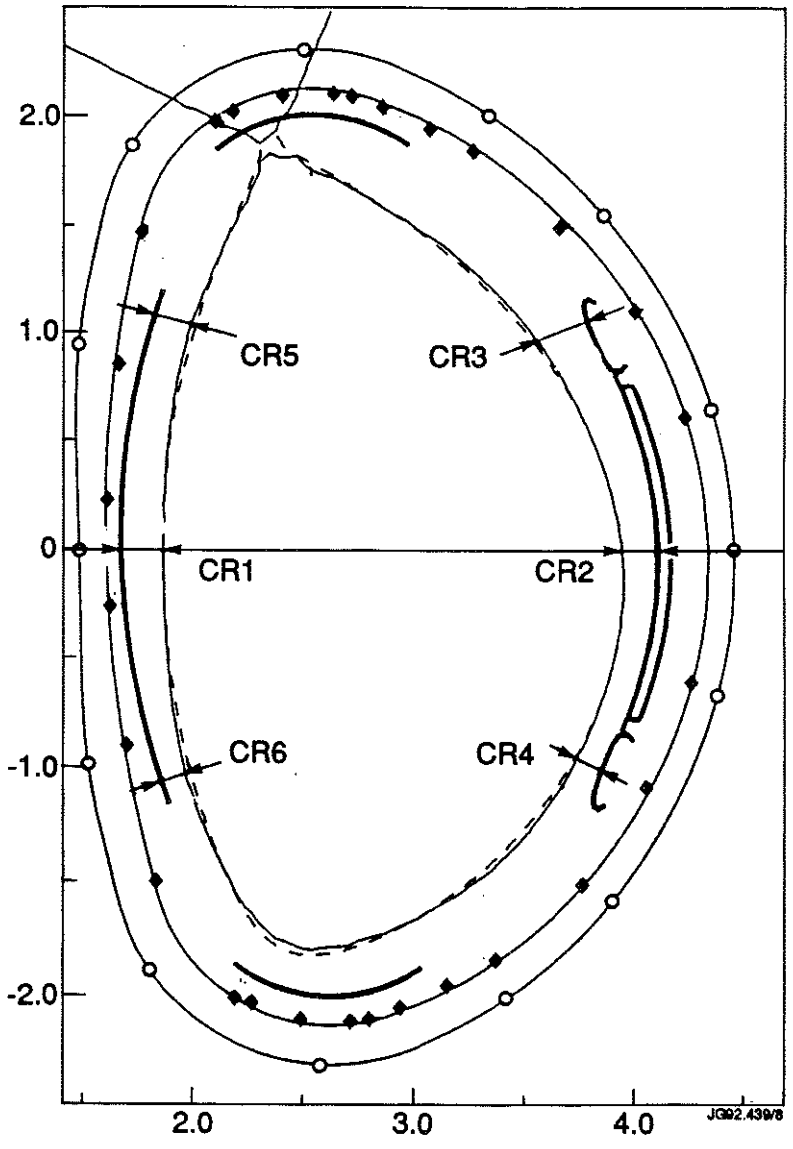

Fig. 1 a) XLOC boundary (solid curve) superimposed on the IDENTC boundary for a single null X-point configurations. Also shown are the distances CR1 - CR6 to various components of the vessel.

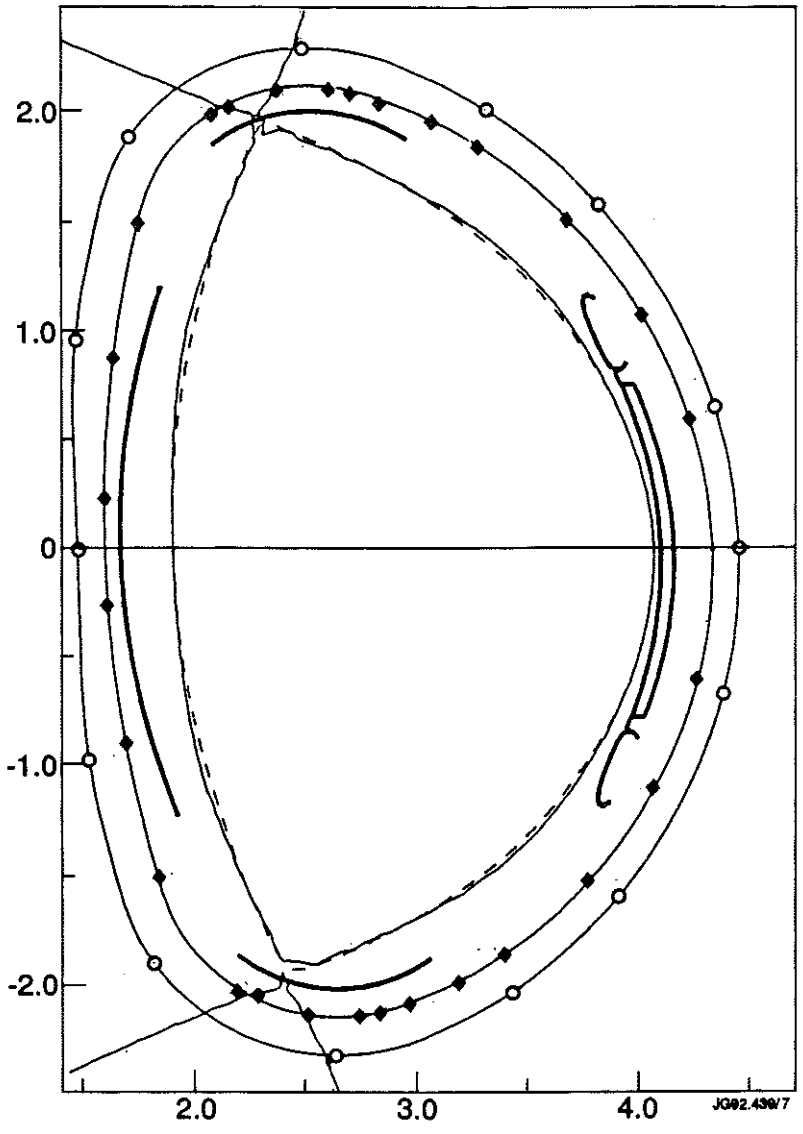

b) XLOC boundary (solid curve) superimposed on the IDENTC boundary for a double null X-point configuration.

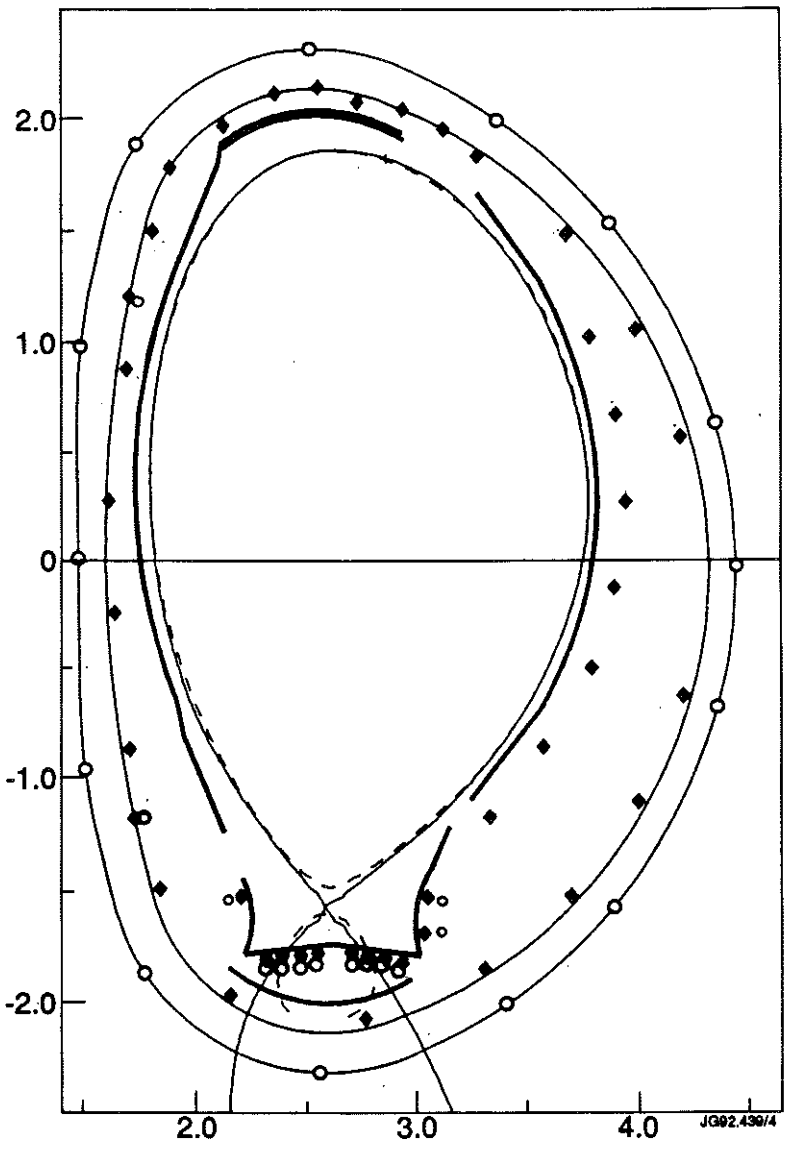

Fig. 2 XLOC boundary (solid curve) superimposed on the EFITJ boundary for a 5 MA fat pumped divertor configuration.

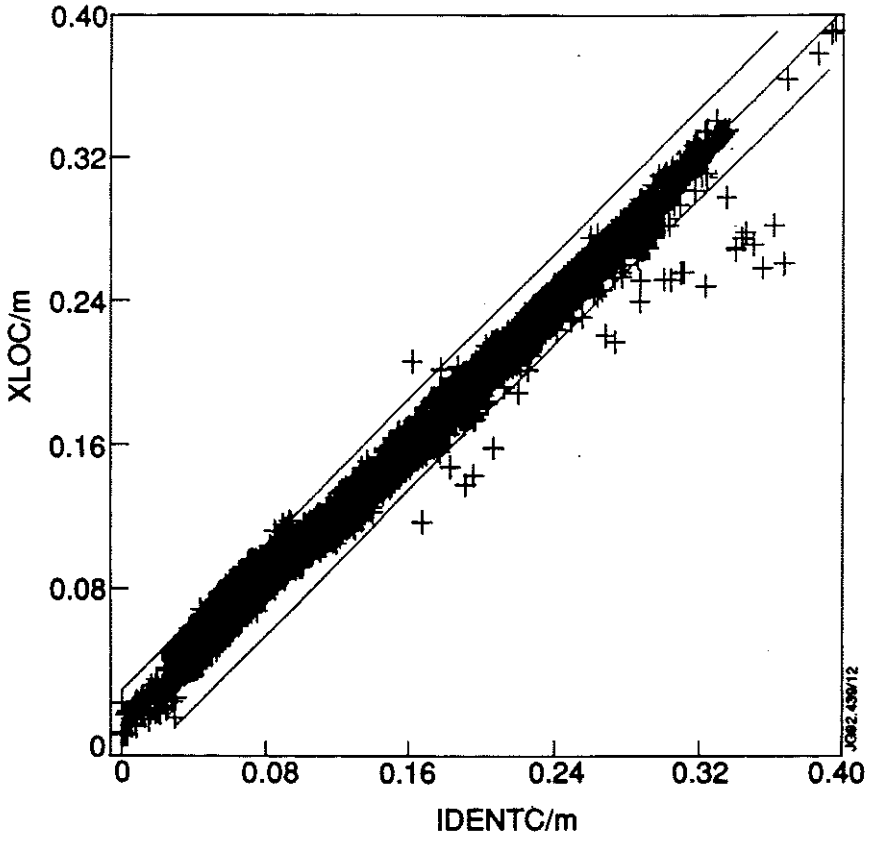

Fig. 3 a) The plasma inner-wall distance from XLOC versus the corresponding IDENTC distance for pulses during the 1990 to 1991 JET campaigns.

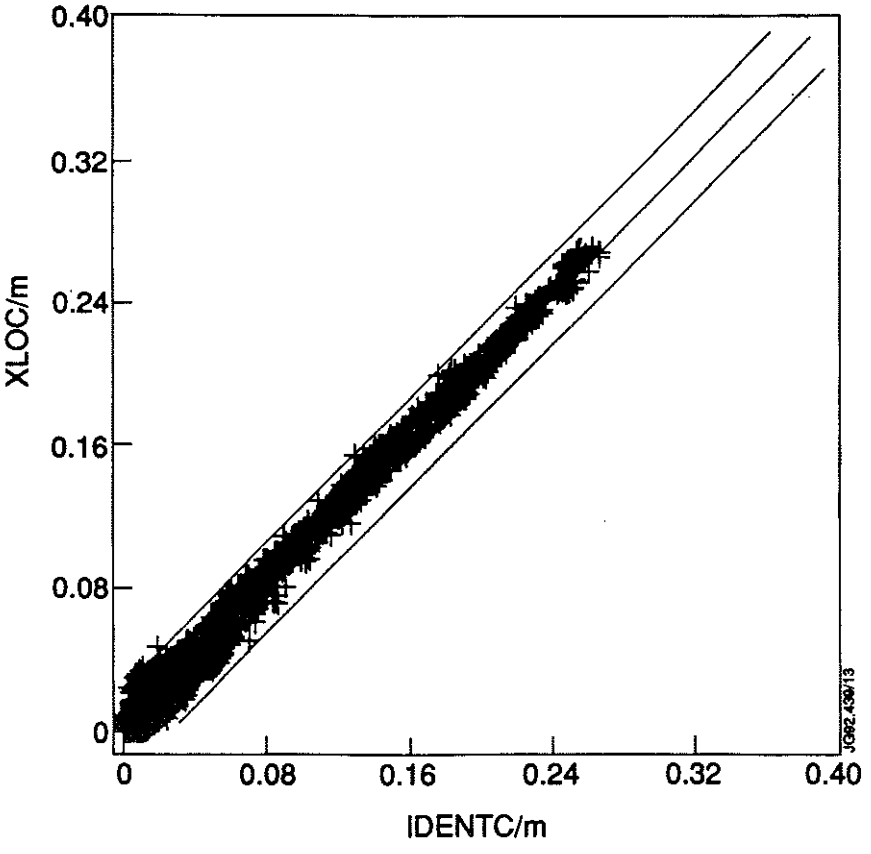

b) The plasma RF-antenna distance from XLOC versus the corresponding IDENTC distance for pulses during the 1990 to 1991 JET campaigns.

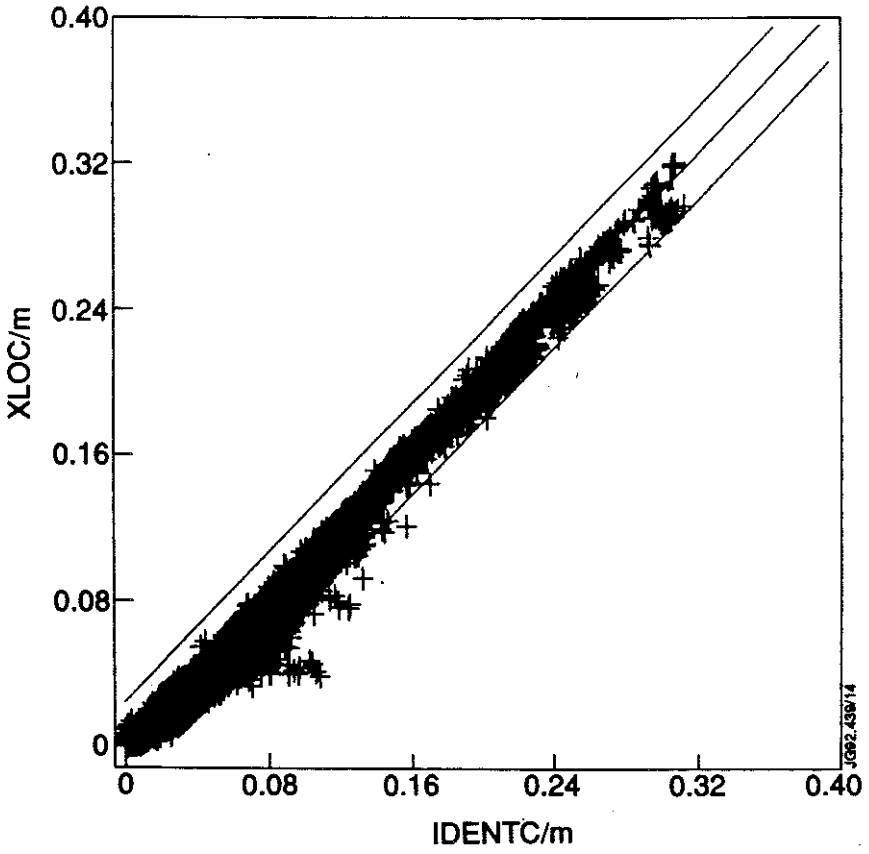

c) The plasma upper-belt distance from XLOC versus the corresponding IDENTC distance for pulses during the 1990 to 1991 JET campaigns.

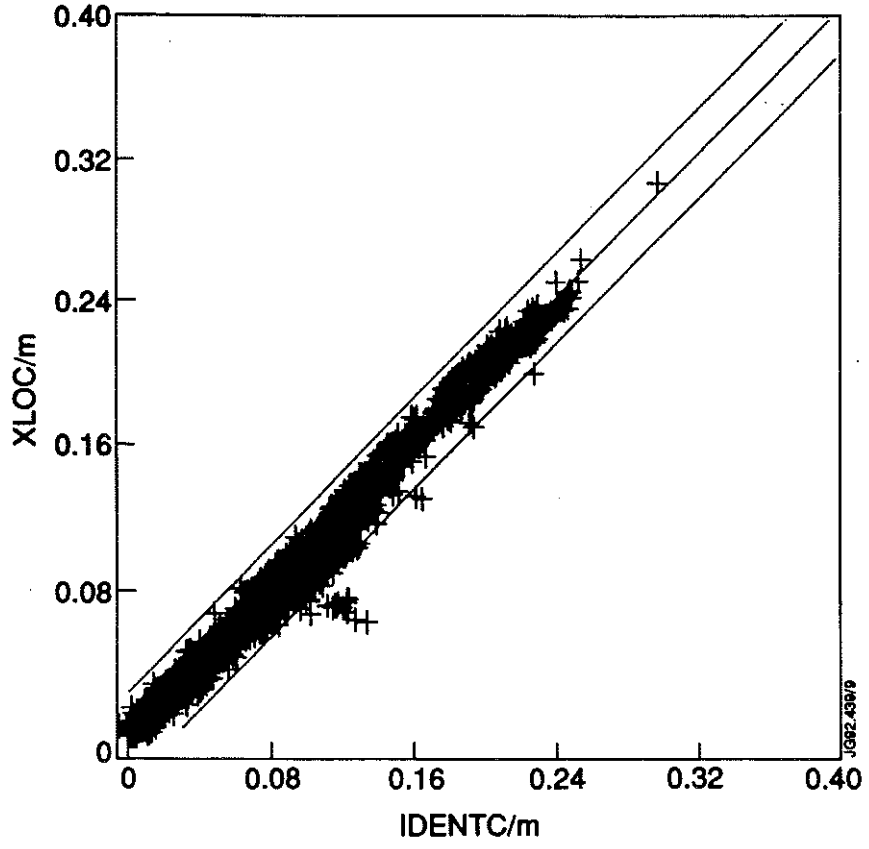

d) The plasma lower-belt distance from XLOC versus the corresponding IDENTC distance for pulses during the 1990 to 1991 JET campaigns.

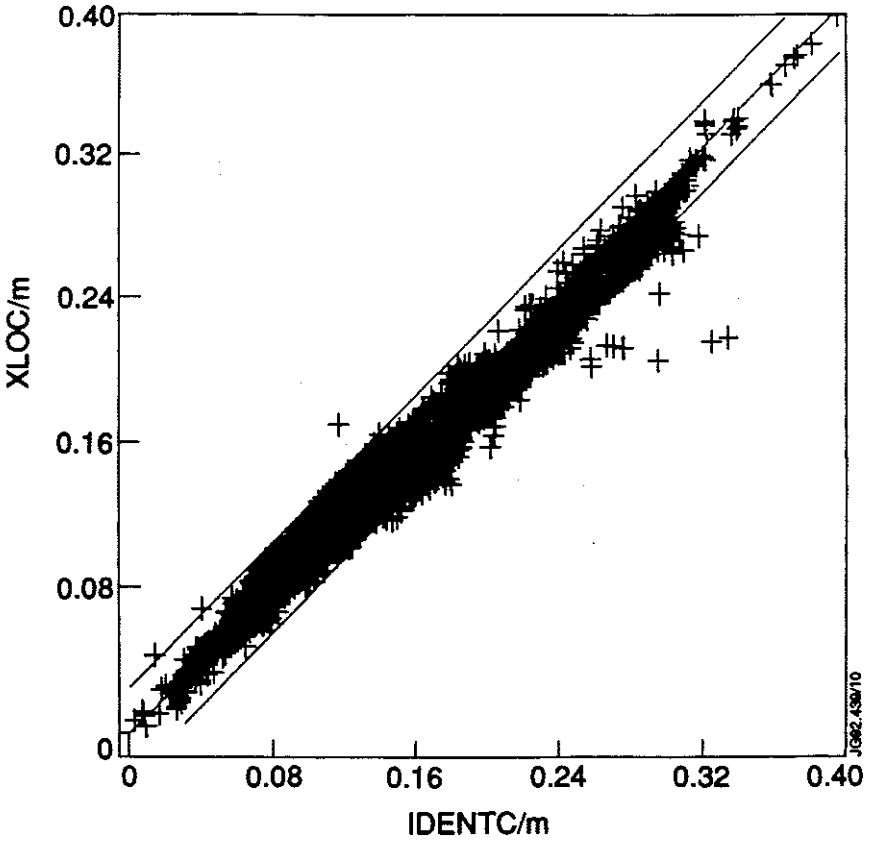

e) The plasma upper inner wall distance from XLOC versus the corresponding IDENTC distance for pulses during the 1990 to 1991 JET campaigns.

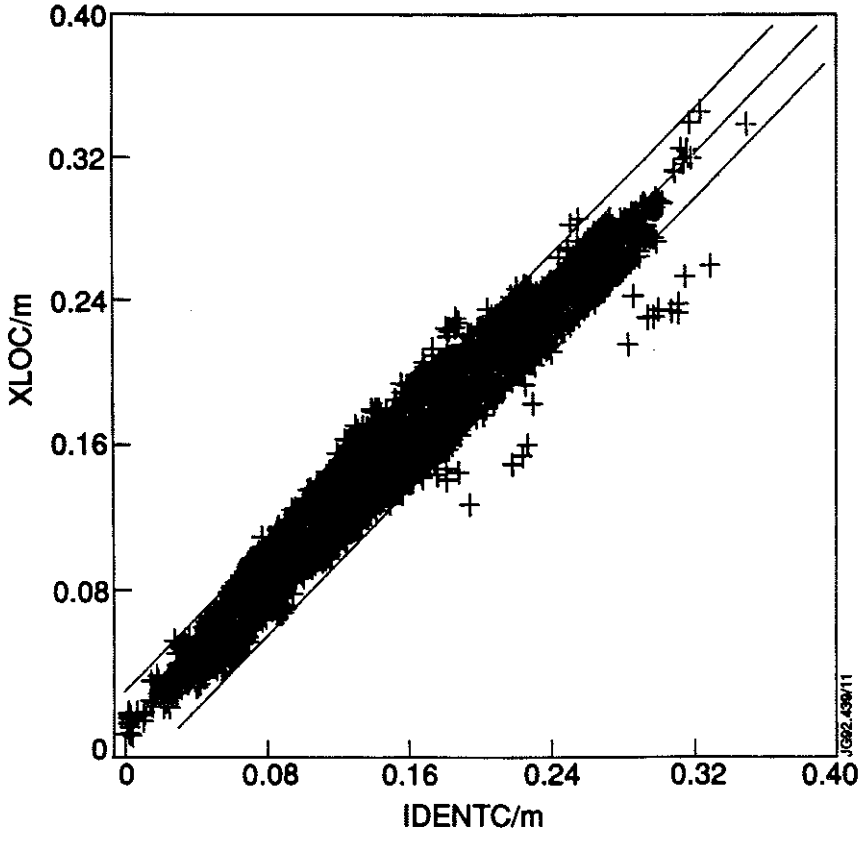

f) The Plasma lower inner wall distance from XLOC versus the corresponding IDENTC distance for pulses during the 1990 to 1991 JET campaigns.

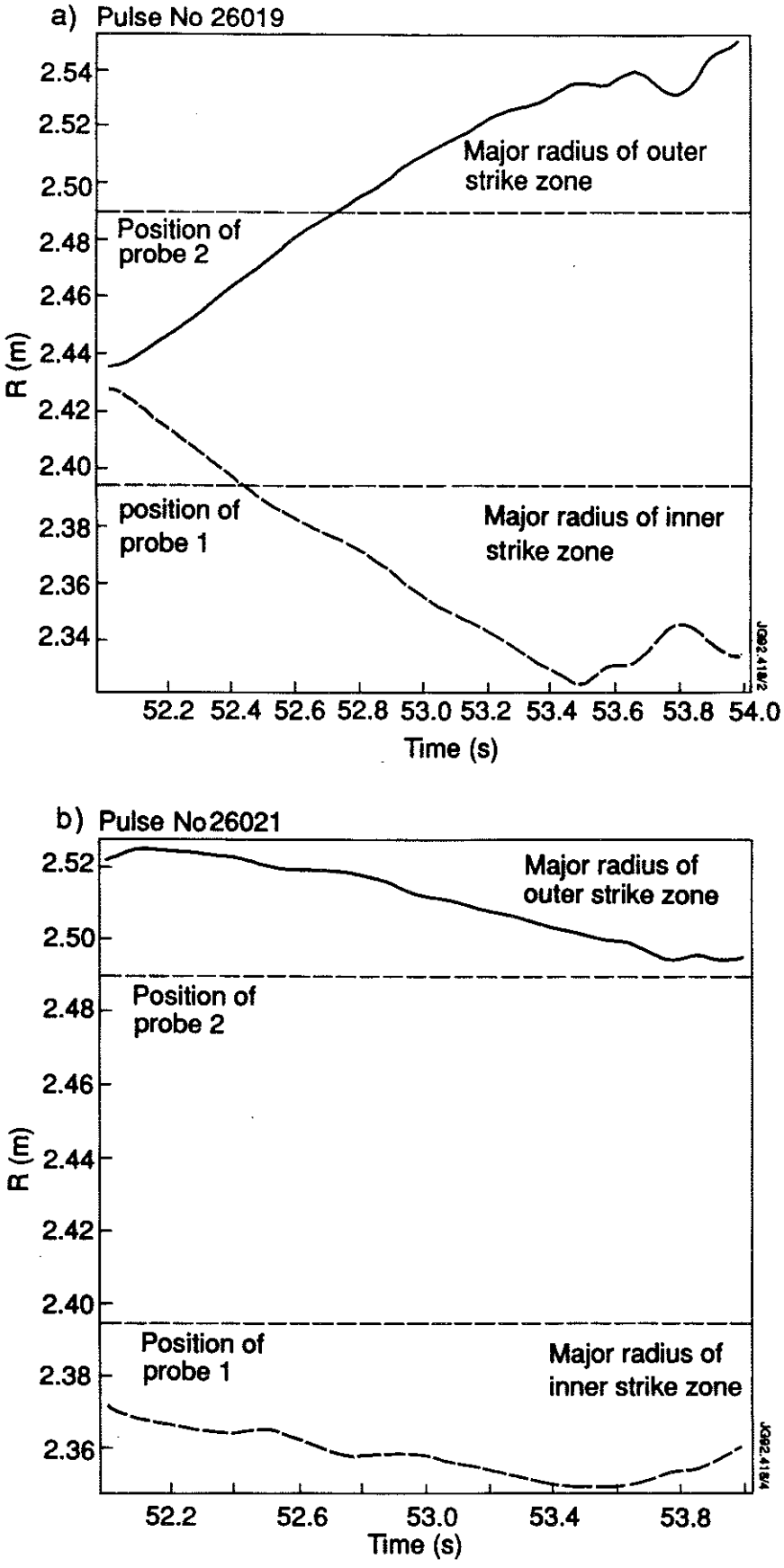

Fig. 4 a,b) The major radius of the inner and outer strike points of the separatrix calculated by XLOC given as a function of time with the positions of Langmuir probes 1 and 2 marked for shots 26019 and 26021 respectively.

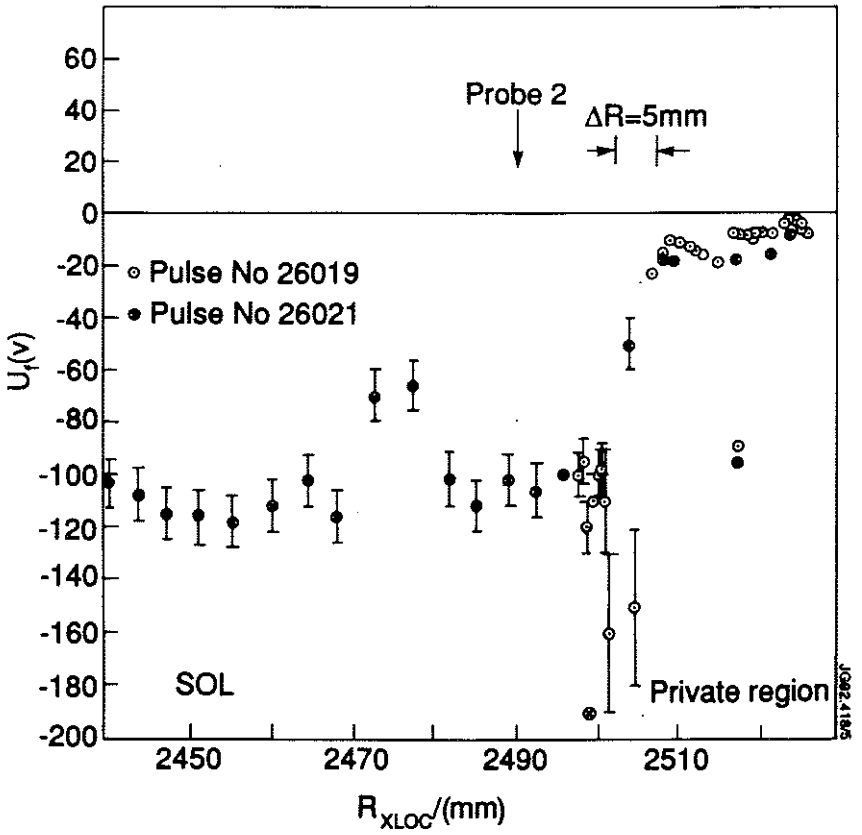

Fig. 5 The floating potential U_f at probe 2 plotted as a function of the position of the outer strike point calculated by XLOC for shots 26019 and 26021.

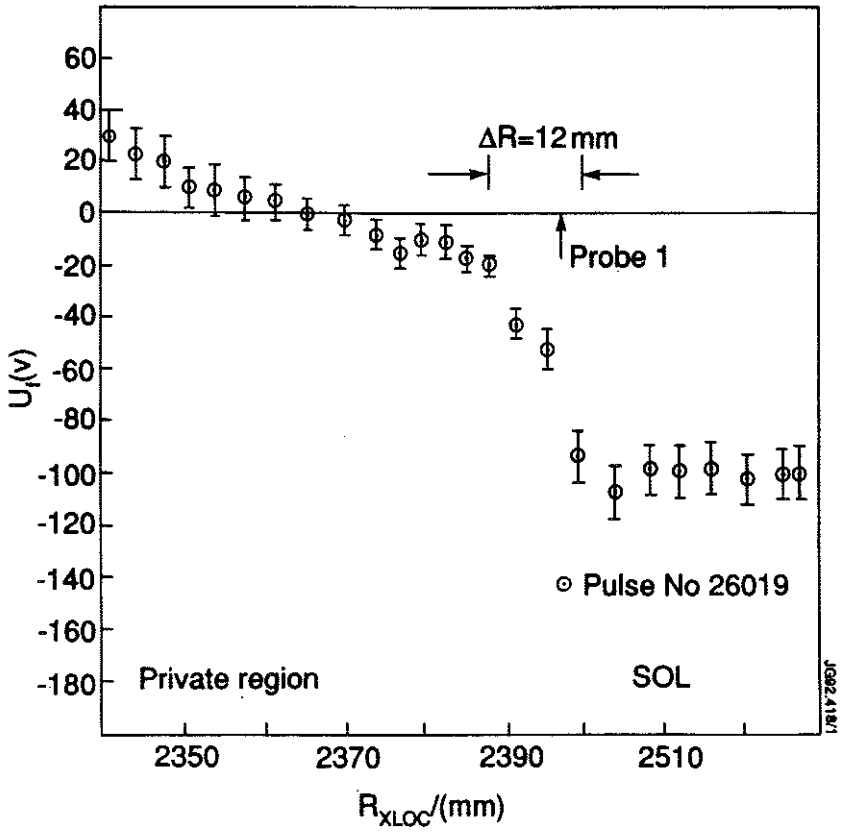

Fig. 6 The floating potential U_f at probe 1 plotted as a function of the position of the inner strike point calculated by XLOC for shot 26019.

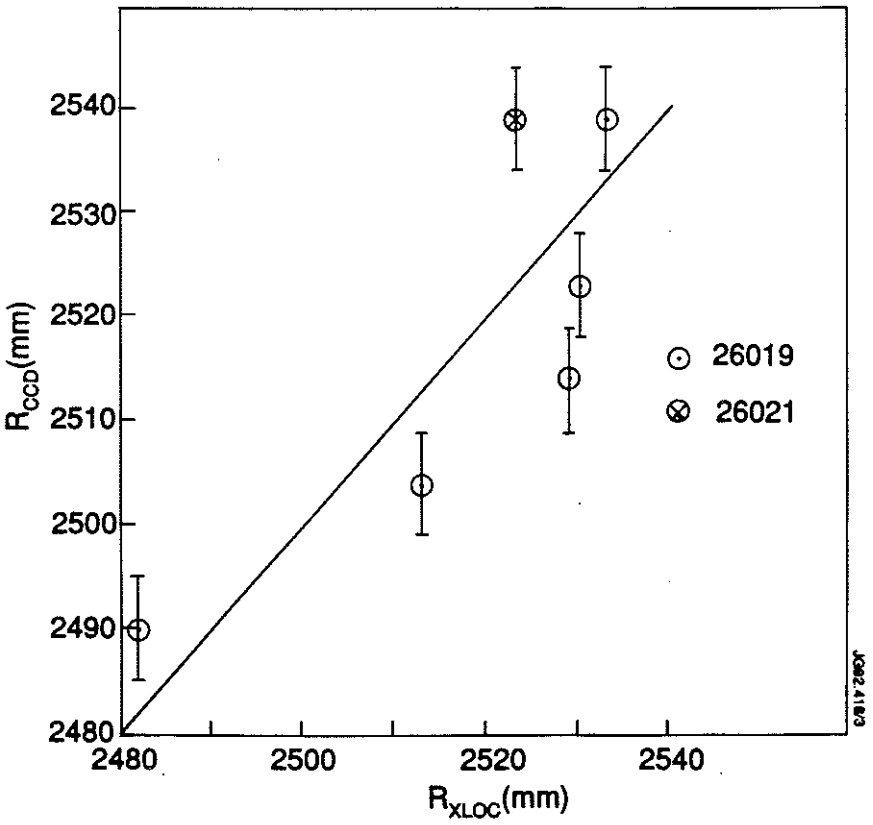

Fig. 7 The location of the outer strike zone determined from the CCD camera recordings versus the calculated outer strike point position from XLOC.

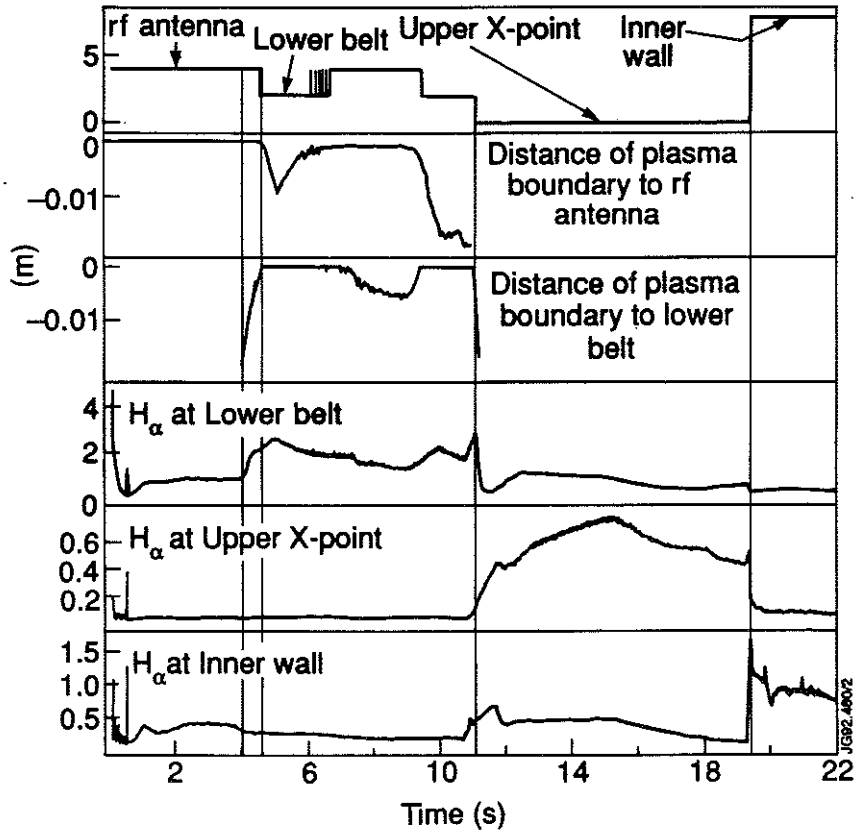

Fig. 8 Comparison of XLOC plasma configuration with spectroscopic measurements.

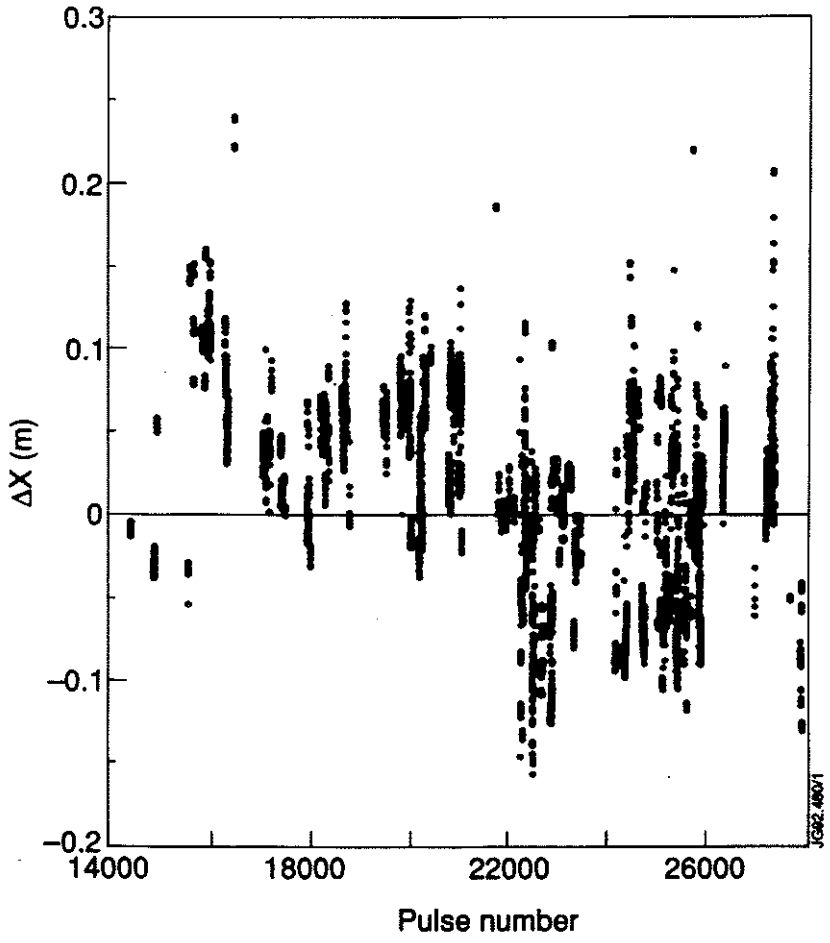

Fig. 9 The distance of the upper X-point from the carbon tiles for H-mode discharges during the 1988 to 1992 JET campaigns. A positive value corresponds to X-points outside the vessel and a negative value to X-points inside the vessel.

Appendix I

THE JET TEAM

JET Joint Undertaking, Abingdon, Oxon, OX14 3EA, U.K.

J.M. Adams[1], B. Alper, H. Altmann, A. Andersen[14], P. Andrew, S.Ali-Arshad, W. Bailey, B. Balet, P. Barabaschi, Y. Baranov, P. Barker, R. Barnsley[2], M. Baronian, D.V. Bartlett, A.C. Bell, G. Benali, P. Bertoldi, E. Bertolini, V. Bhatnagar, A.J. Bickley, D. Bond, T. Bonicelli, S.J. Booth, G. Bosia, M. Botman, D. Boucher, P. Boucquey, M. Brandon, P. Breger, H. Brelen, W.J. Brewerton, H. Brinkschulte, T. Brown, M. Brusati, T. Budd, M. Bures, P. Burton, T. Businaro, P. Butcher, H. Buttgereit, C. Caldwell-Nichols, D.J. Campbell, D. Campling, P. Card, G. Celentano, C.D. Challis, A.V.Chankin[23], A. Cherubini, D. Chiron, J. Christiansen, P. Chuilon, R. Claesen, S. Clement, E. Clipsham, J.P. Coad, I.H. Coffey[24], A. Colton, M. Comiskey[4], S. Conroy, M. Cooke, S. Cooper, J.G. Cordey, W. Core, G. Corrigan, S. Corti, A.E. Costley, G. Cottrell, M. Cox[7], P. Crawley, O. Da Costa, N. Davies, S.J. Davies[7], H. de Blank, H. de Esch, L. de Kock, E. Deksnis, N. Deliyanakus, G.B. Denne-Hinnov, G. Deschamps, W.J. Dickson[19], K.J. Dietz, A. Dines, S.L. Dmitrenko, M. Dmitrieva[25], J. Dobbing, N. Dolgetta, S.E. Dorling, P.G. Doyle, D.F. Düchs, H. Duquenoy, A. Edwards, J. Ehrenberg, A. Ekedahl, T. Elevant[11], S.K. Erents[7], L.G. Eriksson, H. Fajemirokun[12], H. Falter, J. Freiling[15], C. Froger, P. Froissard, K. Fullard, M. Gadeberg, A. Galetsas, L. Galbiati, D. Gambier, M. Garribba, P. Gaze, R. Giannella, A. Gibson, R.D. Gill, A. Girard, A. Gondhalekar, D. Goodall[7], C. Gormezano, N.A. Gottardi, C. Gowers, B.J. Green, R. Haange, A. Haigh, C.J. Hancock, P.J. Harbour, N.C. Hawkes[7], N.P. Hawkes[1], P. Haynes[7], J.L. Hemmerich, T. Hender[7], J. Hoekzema, L. Horton, J. How, P.J. Howarth[5], M. Huart, T.P. Hughes[4], M. Huguet, F. Hurd, K. Ida[18], B. Ingram, M. Irving, J. Jacquinot, H. Jaeckel, J.F. Jaeger, G. Janeschitz, Z. Jankowicz[22], O.N. Jarvis, F. Jensen, E.M. Jones, L.P.D.F. Jones, T.T.C. Jones, J-F. Junger, F. Junique, A. Kaye, B.E. Keen, M. Keilhacker, W. Kerner, N.J. Kidd, R. Konig, A. Konstantellos, P. Kupschus, R. Lässer, J.R. Last, B. Laundy, L. Lauro-Taroni, K. Lawson[7], M. Lennholm, J.Lingertat[13], R.N. Litunovski, A. Loarte, R. Lobel, P. Lomas, M. Loughlin, C. Lowry, A.C. Maas[15], B. Macklin, C.F. Maggi[16], G. Magyar, V. Marchese, F. Marcus, J. Mart, D. Martin, E. Martin, R. Martin-Solis[8], P. Massmann, G. Matthews, H. McBryan, G. McCracken[7], P. Meriguet, P. Miele, S.F. Mills, P. Millward, E. Minardi[16], R. Mohanti[17], P.L. Mondino, A. Montvai[3], P. Morgan, H. Morsi, G. Murphy, F. Nave[27], S. Neudatchin[23], G. Newbert, M. Newman, P. Nielsen, P. Noll, W. Obert, D. O'Brien, J. O'Rourke, R. Ostrom, M. Ottaviani, S. Papastergiou, D. Pasini, B. Patel, A. Peacock, N. Peacock[7], R.J.M. Pearce, D. Pearson[12], J.F. Peng[26], R. Pepe de Silva, G. Perinic, C. Perry, M.A. Pick, J. Plancoulaine, J-P. Poffé, R. Pohlchen, F. Porcelli, L. Porte[19], R. Prentice, S. Puppin, S. Putvinskii[23], G. Radford[9], T. Raimondi, M.C. Ramos de Andrade, M. Rapisarda[29], P-H. Rebut, R. Reichle, S. Richards, E. Righi, F. Rimini, A. Rolfe, R.T. Ross, L. Rossi, R. Russ, H.C. Sack, G. Sadler, G. Saibene, J.L. Salanave, G. Sanazzaro, A. Santagiustina, R. Sartori, C. Sborchia, P. Schild, M. Schmid, G. Schmidt[6], H. Schroepf, B. Schunke, S.M. Scott, A. Sibley, R. Simonini, A.C.C. Sips, P. Smeulders, R. Smith, M. Stamp, P. Stangeby[20], D.F. Start, C.A. Steed, D. Stork, P.E. Stott, P. Stubberfield, D. Summers, H. Summers[19], L. Svensson, J.A. Tagle[21], A. Tanga, A. Taroni, C. Terella, A. Tesini, P.R. Thomas, E. Thompson, K. Thomsen, P. Trevalion, B. Tubbing, F. Tibone, H. van der Beken, G. Vlases, M. von Hellermann, T. Wade, C. Walker, D. Ward, M.L. Watkins, M.J. Watson, S. Weber[10], J. Wesson, T.J. Wijnands, J. Wilks, D. Wilson, T. Winkel, R. Wolf, D. Wong, C. Woodward, M. Wykes, I.D. Young, L. Zannelli, A. Zolfaghari[28], G. Zullo, W. Zwingmann.

PERMANENT ADDRESSES

1. UKAEA, Harwell, Didcot, Oxon, UK.
2. University of Leicester, Leicester, UK.
3. Central Research Institute for Physics, Budapest, Hungary.
4. University of Essex, Colchester, UK.
5. University of Birmingham, Birmingham, UK.
6. Princeton Plasma Physics Laboratory, New Jersey, USA.
7. UKAEA Culham Laboratory, Abingdon, Oxon, UK.
8. Universidad Complutense de Madrid, Spain.
9. Institute of Mathematics, University of Oxford, UK.
10. Freien Universität, Berlin, F.R.G.
11. Royal Institute of Technology, Stockholm, Sweden.
12. Imperial College, University of London, UK.
13. Max Planck Institut für Plasmaphysik, Garching, FRG.
14. Risø National Laboratory, Denmark.
15. FOM Instituut voor Plasmafysica, Nieuwegein, The Netherlands.
16. Dipartimento di Fisica, University of Milan, Milano, Italy.
17. North Carolina State University, Raleigh, NC, USA
18. National Institute for Fusion Science, Nagoya, Japan.
19. University of Strathclyde, 107 Rottenrow, Glasgow, UK.
20. Institute for Aerospace Studies, University of Toronto, Ontario, Canada.
21. CIEMAT, Madrid, Spain.
22. Institute for Nuclear Studies, Otwock-Swierk, Poland.
23. Kurchatov Institute of Atomic Energy, Moscow, USSR
24. Queens University, Belfast, UK.
25. Keldysh Institute of Applied Mathematics, Moscow, USSR.
26. Institute of Plasma Physics, Academica Sinica, Hefei, P. R. China.
27. LNETI, Savacem, Portugal.
28. Plasma Fusion Center, M.I.T., Boston, USA.
29. ENEA, Frascati, Italy.

At 1st July, 1992